J. Mol. Biol. (1997) 268, 468–481

JMB

Solution Structure of Recombinant Human Interleukin-6

Guang-Yi Xu[1], Hsiang-Ai Yu[1], Jin Hong[1], Mark Stahl[1], Thomas McDonagh[1], Lewis E. Kay[2] and Dale A. Cumming[1]*

[1]*Small Molecule Drug Discovery, Genetics Institute 87 Cambridge Park Drive Cambridge, MA 02140, USA*

[2]*Department of Medical Genetics, Biochemistry and Chemistry, University of Toronto, Toronto, Ontario Canada, M5S 1A8*

**Corresponding author*

Interleukin-6 (IL-6) is a 185 amino acid cytokine which exerts multiple biological effects *in vivo* and whose dysregulation underlies several disease processes. The solution structure of recombinant human interleukin-6 has now been determined using heteronuclear three and four-dimensional NMR spectroscopy. The structure of the molecule was determined using 3044 distance and torsion restraints derived by NMR spectroscopy to generate an ensemble of 32 structures using a combined distance geometry/simulated annealing protocol. The protein contains five α-helices interspersed with variable-length loops; four of these helices constitute a classical four-helix bundle with the fifth helix located in the CD loop. There were no distance violations greater than 0.3 Å in any of the final 32 structures and the ensemble has an average-to-the-mean backbone root-mean-square deviation of 0.50 Å for the core four-helix bundle. Although the amino-terminal 19 amino acids are disordered in solution, the remainder of the molecule has a well defined structure that shares many features displayed by other long-chain four-helix bundle cytokines. The high-resolution NMR structure of hIL-6 is used to rationalize available mutagenesis data in terms of a heteromeric receptor complex.

Keywords: cytokine; IL-6; NMR structure; mutagenesis

Introduction

Interleukin-6 (IL-6) is a cytokine originally identified as a T-cell-derived factor regulating B-cell growth and differentiation (Hirano *et al.*, 1986). IL-6 exerts multiple biological effects *in vivo* including the induction of acute phase proteins in liver (Kishimoto, 1989), serving as an autocrine and paracrine growth factor in the pathogenesis of human multiple myeloma (Kawano *et al.*, 1988), and stimulating the recruitment and formation of osteoclasts (Ishimi *et al.*, 1990). IL-6 is an important component of the inflammatory cascade. The proinflammatory cytokines IL-1 and tumor necrosis factor-α (TNF-α) markedly stimulate the production of IL-6 (Van Damme *et al.*, 1987; Mawatari *et al.*, 1989) while neutralizing antibodies to IL-6 protect mice from lethal challenges of *Escherichia coli* or TNF (Starnes *et al.*, 1990). Moreover, dysregulation of IL-6 production has been implicated in a variety of inflammatory/autoimmune disease states including rheumatoid arthritis, cardiac myxoma, Castleman's disease, and mesangial proliferative glomerulonephritis (reviewed by Hirano *et al.*, 1990).

The pleiotropic biological effects of IL-6 are mediated through the generation of a heterotrimeric receptor complex formed by the engagement of IL-6 with an IL-6-specific receptor subunit (IL-6Rα) followed by recruitment of an additional target-cell protein, gp130 (Kishimoto *et al.*, 1992). While both IL-6Rα and gp130 are integral membrane proteins with a single transmembrane domain, activation of intracellular signaling pathways is dependent upon association of an IL-6/IL-6Rα complex with gp130 (Taga *et al.*, 1989).

Abbreviations used: G-CSF, granulocyte colony stimulating factor; M-CSF, macrophage colony stimulating factor; LIF, leukemia inhibitory factory; OSM, oncostatin M; TNF-α, tumor necrosis factor-α; CNTF, ciliary neurotrophic factor; EPO, erythropoietin; IL-6, interleukin-6; GH, growth hormone; NOE, nuclear Overhauser effect; NOESY, nuclear Overhauser effect spectroscopy; HMQC, heteronuclear multiple-quantum coherence; HSQC, heteronuclear single-quantum coherence; RMSD, root-mean-square deviation; Mes, 2-(*N*-morpholino)ethanesulfonic acid; TPPI, time-proportional phase incrementation; CCJ, $^{13}C-^{13}C$ *J* coupling; 2D, two-dimensional; 3D, three-dimensional; 4D, four-dimensional; IFN-β, interferon-β.

0022–2836/97/170468–14 $25.00/0/mb970933

Specifically, IL-6/IL-6Rα induces disulfide-linked homodimerization of gp130 which alone leads to activation of the JAK/STAT signaling pathway (Murakami *et al.*, 1993; Ivashkiv, 1995; Paonessa *et al.*, 1995).

Thus the final receptor complex, which can mediate signal transduction, is believed to be hexameric and composed of two molecules each of IL-6, IL-6Rα, and gp130 with intermolecular contacts between all three components (Murakami *et al.*, 1993; Ward *et al.*, 1994; Paonessa *et al.*, 1995). Residues in IL-6 critical for specific binding to IL-6Rα or gp130 have been identified by site-directed mutagenesis (Savino *et al.*, 1993; 1994b; Paonessa *et al.*, 1995). Several other cytokines, including leukemia inhibitory factor (LIF), oncostatin M (OSM), and ciliary neurotrophic factor (CNTF), also employ receptors that are members of the hematopoietin receptor superfamily and associate with gp130 (or gp130-like molecules) for subsequent signal transduction (Kishimoto *et al.*, 1992; Davis *et al.*, 1993; Mott & Campbell, 1995).

IL-6 is a member of a family of cytokines/growth factors, which are believed to share a common topological fold despite limited amino acid sequence homology. All of these cytokines are believed to have three-dimensional structures comprised of a core bundle of four α-helices connected by variable-length loops. Together with, *inter alia*, IL-11, IL-12, and erythropoietin (EPO), IL-6 has been classified into a subfamily of ''long-chain'' four-helix bundles which share several structural features including overall polypeptide chain length, average length of helices, and characteristic packing of the antiparallel helical pairs (Sprang & Bazan, 1993). These predicted structural features for long-chain four-helix bundles have been largely confirmed by recent NMR and X-ray crystallographic studies of growth hormone (GH), G-CSF, LIF, and CNTF (Zink *et al.*, 1994; Hill *et al.*, 1993; McDonald *et al.*, 1995; Robinson *et al.*, 1994; Ultsch *et al.*, 1994). However, the structure of IL-6 has not been reported. We have pursued the determination of the three-dimensional solution structure of IL-6 by multidimensional, heteronuclear NMR spectroscopy. We have reported on the sequence-specific assignments, secondary structure analysis, and overall topological fold for IL-6 (Xu *et al.*, 1996), providing experimental confirmation for at least some of the structural predictions made for IL-6. Here, we report the high resolution NMR solution structure for IL-6, which together with another report of the X-ray structure determination (Somers *et al.*, 1997), provides the first experimental tertiary structure information on IL-6.

Results

Experimental restraints

Essentially all restraints are localized to residues 20 to 185; we have reported that the amino-terminal 19 residues of IL-6 are extremely flexible, as evidenced by observed ^{15}N T_2 values (Xu *et al.*, 1996), and thus fail to yield any restraints useful for 3D structure determination. A total of 2961 interproton distance restraints were obtained from three-dimensional (3D) and four-dimensional (4D) NMR spectra of either singly (^{15}N) or doubly labeled (^{15}N, ^{13}C) IL-6. This set is composed of 897 intraresidue, 835 sequential, 648 medium-range, and 443 long-range restraints, yielding an average of 17 distance restraints-per-residue. Included within this set are 138 hydrogen-bonding restraints derived from NMR observation of 69 backbone amide hydrogen atoms which showed slow exchange with ^2H_2O and were assigned hydrogen-bonding partners in α-helical segments in conjunction with local nuclear Overhauser enhancement (NOE) patterns.

In addition, other experimental restraints were employed in the structure determination. A total of 83 dihedral angles were derived from $^3J_{HN,H^\alpha}$ values obtained as described in Methods. Obtaining a greater number of angular restraints was precluded largely by the lack of spectral dispersion of this four-helix bundle. Only relatively few stereospecific assignments could be made largely due to the motional characteristics of IL-6 (Xu *et al.*, 1996). For example, average ^{15}N T_2 values observed in the core region of IL-6 were about 40 ms; such behavior results in very poor magnetization transfer *via* scalar coupling in NMR experiments. This characteristic of IL-6 made resonance assignment difficult, and made obtaining stereospecific assignments for methylene protons impossible. However, due to the relatively fast rotational behavior of methyl groups located at the terminus of side-chains and their consequently improved spectral traits, some stereospecific assignments were made for certain well-resolved leucine δ-methyl moieties. In total, stereospecific assignments for the δ-methyl groups of ten out of 23 leucine residues were obtained as described in Methods. While few in number, these assignments proved to be especially valuable, since these residues were found buried within the folded core of IL-6 and thus provided many stereospecific interhelical NOEs.

Calculations

A family of 75 embedded substructures were generated using distance geometry (Brünger, 1993) followed by simulated annealing, regularization, and refinement (Nilges *et al.*, 1988). An iterative procedure was used in the latter three steps to successively introduce an increasing number of NOE distance restraints. The procedure also examines any NOE violations in the family of interim structures and attempts to adjust their classification (strong, medium or weak) to relieve violations. This process was repeated until all 2961 NOE distance (including 138 hydrogen bond) and 83 torsion angle restraints were used, producing a set of structures that did not exhibit either any NOE distance violation greater than 0.3 Å or any torsional

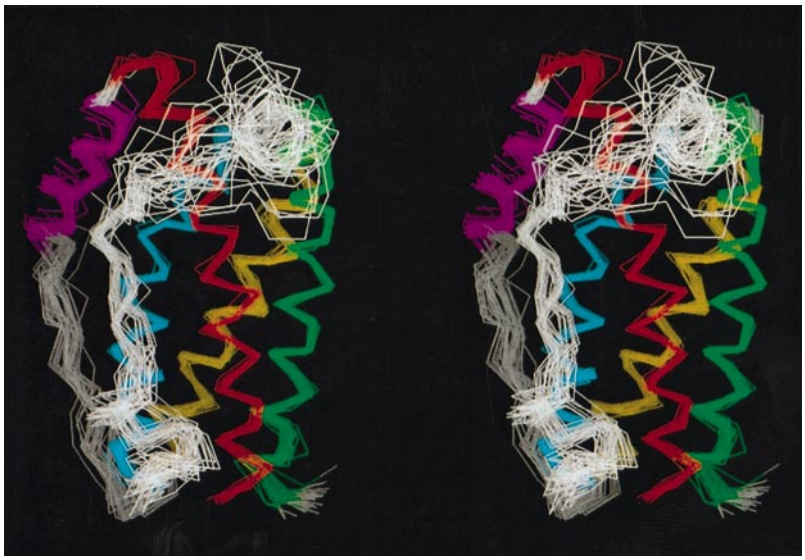

Figure 1. Stereo diagram illustrating best-fit superpositions of the C^{α} traces of the 32 structures of IL-6 in the final ensemble. The color coding scheme is as follows: Helices A to E are shown, respectively: green, blue, yellow, red, and magenta. The AB and CD crossover loops are white.

angle violation greater than five degrees. Further refinement of the set of structures was performed by utilizing the Aqua/Procheck-NMR suite of programs (Laskowski *et al*., 1996) to identify any NOE distance violations less than 0.3 Å common to the entire ensemble. Fourteen such restraints were identified and reclassified; a final round of simulated annealing and regularization was then performed.

A final ensemble of 32 structures was obtained. After superimposing all main-chain N, C^{α} and C atoms of the 105 residues defining the core four-helix bundle (Figure 1; helix A, 21 to 47 shown in green; helix B, 81 to 105 shown in blue ; helix C, 109 to 131 shown in yellow; helix D, 156 to 185 shown in red), the average structure was calculated by averaging over the Cartesian coordinates of the ensemble. The average structure was further subjected to 1000 steps of Powell minimization using X-PLOR (Brünger, 1993). Assignment of the helical residues, including residues 143 to 154 for helix E, is based on an evaluation of the average structure using the program Procheck 3.0 (Laskowski *et al*., 1993) to include all residues with secondary structural assignments of ''H'' or ''h''. Coordinates for all members of the ensemble and the averaged structure have been deposited with the Brookhaven Protein Data Bank (accession no. 1IL6).

Description of the NMR-derived structures

The overall topology for IL-6 in solution is that of a long-chain, up-up-down-down left-handed four-helix bundle with long loops connecting helices A and B as well as C and D, consistent with previous secondary structure analysis and evaluation of a limited set of NOEs (Xu *et al*., 1996). Figure 1 shows a stereo diagram of the C^{α} traces of the 32 structures constituting the final ensemble and illustrates the quality of the ensemble. The precision of the final set is striking, particularly in terms of the packing and orientation in the core (A to D) helices. The root-mean-square difference (RMSD) from the average structure of main-chain atoms in the 32 four-helix cores is only 0.50 Å; the RMSD for all non-hydrogen atoms in the core region increases to 1.0 Å. Most of the observed conformational variability among the 32 structures is localized to the crossover loop regions (shown in white), particularly at the amino-terminal portion of the AB loop. The RMSD from the average structure for all main-chain atoms in the 32 structures is 1.1 Å and for all non-hydrogen atoms is 1.6 Å.

The quality of the high resolution NMR structures can be assessed more quantitatively in several ways. For example, the distribution of NOE restraints over the protein and their correlation to

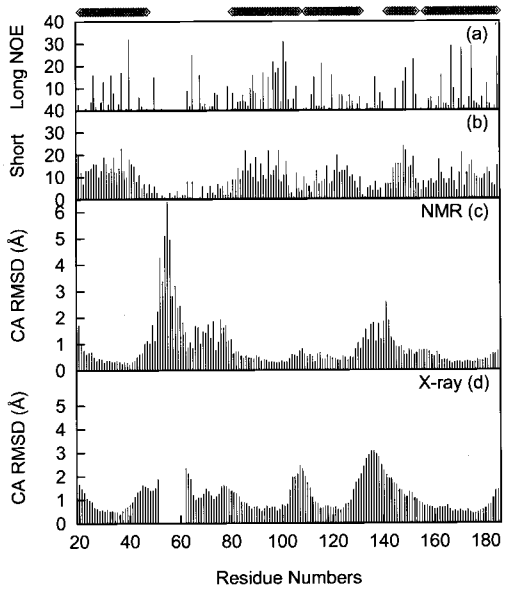

Figure 2. Per-residue structural statistics from the ensemble of 32 NMR-derived structures. (a) and (b), Number of long and short-range NOEs, respectively, per residue; (c) and (d), C^{α} RMSD distributions for the NMR and X-ray (Somers *et al*., 1997) structures of IL-6.

Table 1. Structural, energetic statistics and atomic RMSDs

A. *Structural and energetic statistics*

	⟨SA⟩	(SA)r
RMSD from exptl distance restraints (Å)		
All (2961)	0.0211± 0.0011	0.0203
Interresidue sequential ($\|i-j\|=1$) (835)	0.0227 ± 0.0016	0.0229
Interresidue short-range ($1<\|i-j\|\leqslant 5$) (648)	0.0231 ± 0.0022	0.0213
Interresidue long-range ($\|i-j\|>5$) (443)	0.0231 ± 0.0029	0.0205
Intraresidue (897)	0.0119 ± 0.0017	0.0132
H-bonds (138)	0.0346 ± 0.0027	0.0322
RMSD from exptl dihedral restraints (deg.) (83)	0.4302 ± 0.0834	0.3965
RMSD from idealized covalent geometry		
Bonds (Å) (2697)	0.0029 ± 0.0002	0.003
Angles (deg.) (4885)	0.4963 ± 0.0168	0.471
Impropers (deg.) (1341)	0.3867 ± 0.0197	0.371
Energetics		
E_{total} (kcal mol^{-1})	369 ± 31	334
E_{repel} (kcal mol^{-1})	66 ± 9	60
E_{NOE} (kcal mol^{-1})	66 ± 7	61
E_{cdih} (kcal mol^{-1})	1.0 ± 0.4	0.8
E_{bond} (kcal mol^{-1})	23 ± 2	19
E_{angle} (kcal mol^{-1})[b]	184 ± 13	165
$E_{improper}$ (kcal mol^{-1})	31 ± 3	28
E_{LJ} (kcal mol^{-1})[a]	−328 ± 44	−393

B. *Non-hydrogen atomic RMSDs* (Å)[b]

	Residues 20-185		Secondary structure[c]	
	Backbone atoms	All atoms	Backbone atoms	All atoms
⟨SA⟩ *versus* SA	1.13 ± 0.32	1.61 ± 0.30	0.50 ± 0.08	1.01 ± 0.08
⟨SA⟩ *versus* (SA)r	1.19 ± 0.39	1.76 ± 0.39	0.53 ± 0.08	1.12 ± 0.10
(SA)r *versus* SA	0.43	0.74	0.19	0.48
SA *versus* X-ray	1.57	2.02	1.30	1.83
(SA)r *versus* X-ray	1.62	2.16	1.35	1.93
⟨SA⟩ *versus* X-ray	1.76 ± 0.09	2.38 ± 0.08	1.40 ± 0.09	2.07 ± 0.10

The NMR structures are denoted as follows: ⟨SA⟩ are the final 32 ensemble structures; SA is the mean structure obtained from averaging the Cartesian coordinates of individual ensemble members; and (SA)r is the minimized average structure obtained by regularization of SA. E_{repel} was calculated using a final force constant of 4.0 kcal mol^{-1} Å^{-4} with van der Waals hard sphere radii scaled by 0.78. E_{NOE} was calculated using a square-well potential with center-averaging and a force constant of 50 kcal mol^{-1} Å^{-2}. E_{cdih} was calculated using a force constant of 200 kcal mol^{-1} rad^{-2}. E_{bond}, E_{angle} and $E_{improper}$ were calculated using force constants of 1000 kcal mol^{-1} Å^{-2}, 500 kcal mol^{-1} rad^{-2} and 500 kcal mol^{-1} rad^{-2}, respectively.

[a] The Lennard-Jones potential is calculated using the default nonbond interaction parameters in CHARMM (Brooks *et al.*, 1983) as implemented in Quanta96 (Molecular Simulation, Inc.); this potential was not used in the refinement protocol.

[b] In all atomic RMS differences calculations, only the backbone atoms (N, C^{α} and C) are included in the least-squared best-fitting.

[c] Core helices A, B, C and D.

RMSD in C^{α}s can be evaluated (Figure 2). Figure 2 (a) and (b) give the number of NOE restraints per residue for long and short-range enhancements (as defined in Table 1), respectively. The five helices from the NMR refinement are shown at the top in the order of A, B, C, E, and D. As one would expect, the number of NOE restraints is greater in helical regions. The characteristic helical periodicity in long-range NOEs is also evident, in particular for helices A, B and D. In order to illustrate the effect of NOE restraints on the quality of the final structure, we show the C^{α} RMSD from the NMR refinement in Figure 2 (c). As expected, there is an inverse correlation such that regions with a higher number of NOE restraints give smaller RMSDs and thus a better-defined structure. Conversely, the region at the beginning of the AB loop has RMSD values significantly higher than all other regions. This is also clearly shown in Figure 1 as the top right corner of the stereo diagram where the white traces span the largest conformational space relative to other parts of the protein. For comparison, we give the C^{α} RMSD calculated from the X-ray refinement (Somers *et al.*, 1997) in Figure 2 (d). The beginning of the AB loop is not evident in the X-ray structure, whereas all other regions show very good positive correlation with that of the NMR data in Figure 2 (c).

The quality of the NMR-derived ensemble can also be assessed energetically. Table 1 lists relevant energetic characteristics. As can be seen, the ensemble appears to be energetically reasonable with acceptable covalent geometry. The values tabulated for the energy-minimized structure reflect one NOE violation greater than 0.3 Å. A Ramachandran ϕ/ψ plot for the energy minimized NMR average structure, as calculated with Procheck 3.0 (Laskowski *et al.*, 1993), shows good clustering of residues in the most favorable α-helical region ($\phi/\psi = -60^{\circ}/-30^{\circ}$), as expected for a four-helical bundle protein (data not shown). A total of 76% of residues are in the most favored regions (A,B,L)

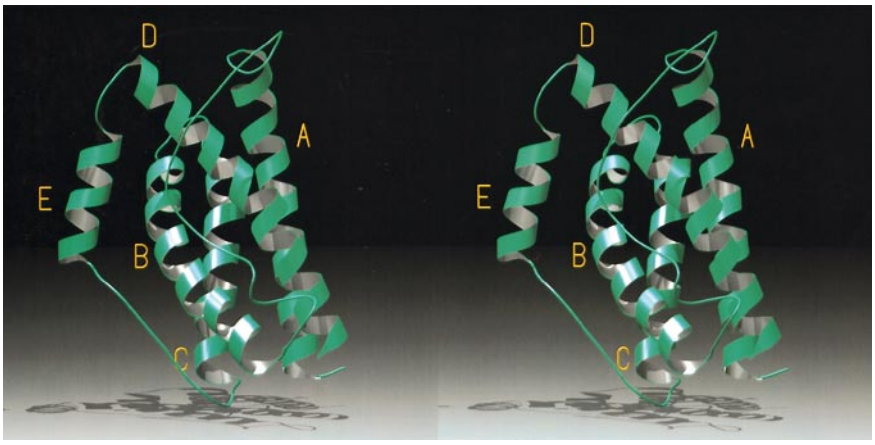

Figure 3. Stereo image of the averaged and minimized NMR structure of IL-6. Only residues 20 to 185 are shown and individual helices are labeled.

while another 19% are in the additional, allowed regions. The remaining 5% of residues fall within generously allowed regions and only one residue (G73) is in a disallowed region.

The high-resolution NMR structures of IL-6 show a number of structural features of interest. The A helix (residues T21 to K47) shows a pronounced ''kink'' (of 34°) starting in the vicinity of residue 42. The existence of a kink correlates with the fact that residues A39 and L40 have some missing $(i,i+4)$ hydrogen bonds characteristic of α-helices. The amino-terminal portion of the AB crossover loop is stabilized by a disulfide bond between C45 and C51 and a hydrogen bond between C45 and E52. The characteristic packing of the AB crossover loop over the top of the D helix and its attached CD loop is evident (Figures 1 and 3; Sprang & Bazan, 1993). The C-terminal portion of

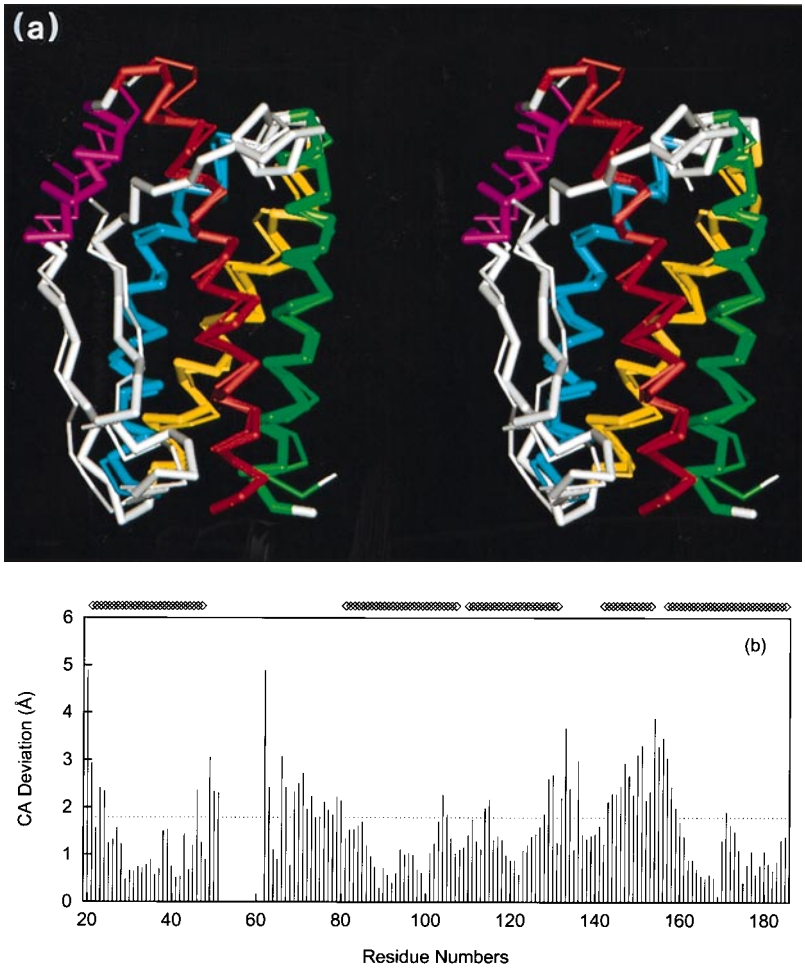

Figure 4. Best-fit superposition of the C^{α} atoms of the X-ray and the restrained minimized averaged NMR structures of IL-6. (a) The color coding scheme is identical to that of Figure 1. The average minimized NMR structure is shown in thick lines while the X-ray structure is shown in thin lines. (b) C^{α}–C^{α} distances after the best-fit superposition.

Table 2. Interhelical and kink angles and interhelical distances for IL-6

A. *Interhelical angles and distances*[a]

Helices	Averaged, minimized NMR		X-ray	
	Angle	Distance	Angle	Distance
A:C	−153.9 ± 2.4	8.6 ± 0.3	−152.7	9.2
A:D	−152.1 ± 1.4	8.4 ± 0.4	−154.5	9.1
B:C	−154.4 ± 1.7	8.7 ± 0.2	−158.2	8.9
B:D	−142.4 ± 1.9	9.0 ± 0.2	−149.1	9.6
A:B	41.6 ± 2.3	12.4 ± 0.2	40.2	13.4
C:D	41.5 ± 2.1	13.2 ± 0.3	35.0	13.5
E:B	−48.3 ± 3.6	11.0 ± 0.3	−49.5	9.6
E:D	−170.9 ± 9.1	9.2 ± 0.5	−170.6	8.9

B. *Intrahelical kink angles*

Helix	Averaged, minimized NMR	X-ray
A	34.0 ± 5.4	15.9
B	31.5 ± 2.9	31.0
C	ND	ND
D	18.0 ± 2.2	7.4

ND, not determined. Angles are in degrees and distances in Å.

[a] The algorithm of Chothia *et al.* (1981) as implemented in CHARMM (Brooks *et al.*, 1983) was used for the analysis.

the AB crossover loop has consecutive five-turn (residues A69 to C74) and three-turn (residues Q76 to F79) elements with additional stabilization through the C74–C84 disulfide bond. A pronounced kink (of 31.5°) in the B helix (residues E81 to R105) is also observed although there is no perturbation of helical (i,$i+4$) hydrogen bonding. Helices B and C (residues E110 to A131) are connected by a five-residue turn. The CD crossover loop has a three-turn element at its amino terminus (A131 to L134) continuing on into an extra-core helix (helix E, residues T143 to A154). The amphipathic E helix is stabilized through extensive side-chain interactions with the core bundle, most particularly with the B helix. These interactions contribute to the E helix being well-defined relative to the rest of the CD loop in the ensemble of NMR structures. The high apparent flexibility in residues E52 to N61 of the AB loop is, in contrast, the result of few side-chain interactions with the core bundle (Figure 1). The D helix (residues Q157 to M185) also shows a slight kink (of 18°) centered roughly in the middle of the helix.

In Figure 4(a), the energy-minimized NMR average structure is compared to that determined by X-ray crystallography (Somers *et al.*, 1997). The color coding corresponds to that used in Figure 1 with the NMR structure in thick lines and the X-ray structure in thin lines. Electron density for residues 52 to 61 in the beginning of the AB loop is not interpretable in the X-ray data. This corresponds to the hypervariable regions in the NMR-derived ensemble as shown in Figure 1. For the most part, the core A, B, C and D helices between the two methods match well with each other (Table 2). Any differences between the structures lie mostly in the loops, at the ends of the helices, and in the E helix. Interestingly, the kinks in A and D helices, observed in the NMR ensemble averaged structure, are not as evident in the X-ray structure. These differences are revealed more quantitatively in Figure 4(b), where the C^{α}–C^{α} distances between the NMR and the X-ray structures are plotted. Observed differences range from 0.1 to 4.9 Å (with an average of 1.8 Å indicated by the dotted line), where larger deviations are mainly localized in the end of helices and in helix E where there is a shift in the whole helix in the X-ray relative to that of the NMR structure. The RMSD in main-chain N, C^{α} and C of the core helices between the averaged NMR and X-ray structures is 1.40 Å as compared to the value of 0.50 Å among the 32 NMR structures. Thus, the structures of IL-6 determined by the two methods agree remarkably well.

The NMR structure also yields interesting insights into the phylogenetics of IL-6. King *et al.* (1995) have previously reported a multiple sequence alignment for IL-6 from nine mammalian species, including human, and showed that all species except mouse and rat show reasonable levels of similarity in their amino acid sequences. It has been suggested that sequence differences in rat and mouse, as compared to the other mammalian species, could account for the inability of murine IL-6 to elicit a response from human cells, while IL-6 from all species can elicit a response from murine cells (see below). A comparable alignment performed as described in Methods shows that 31 amino acid residues are invariant across all species in the residue range L20-M185 (data not shown). Two thirds of these invariant residues fall within helices in human IL-6, four are Cys residues, and the rest lie within the AB loop (Table 3). Evaluation of the alignment in terms of the tertiary structure of human IL-6 indicates that most gaps/insertions fall within two regions: the start of the CD loop (up to start of helix E) or the short turn between helices B and C where an additional Lys residue is

Table 3. Residues absolutely conserved among nine species of IL-6 (residues 20-185)

Residue	Location	Putative role[a]
I30	Helix A	Bundle core packing
I37	Helix A	Bundle core packing
E43	Helix A	
C45	Helix A	Disulfide bonding
C51	AB loop	Disulfide bonding
L58	AB loop	Receptor site III
E60	AB loop	Receptor site III
N61	AB loop	Receptor site III
L63	AB loop	Loop to helix D/E packing
L65	AB loop	Loop to helix B/E packing
P66	AB loop	
D72	AB loop	
C74	AB loop	Disulfide bonding
Q76	AB loop	Receptor site I
N80	AB loop	
C84	Helix B	Disulfide bonding
L85	Helix B	Bundle core packing
G91	Helix B	Bundle core packing
L92	Helix B	Bundle core packing
E94	Helix B	
L99	Helix B	Bundle core packing
L123	Helix C	Bundle core packing
P142	Helix E	
L148	Helix E	Side-chain packing to helix B
W158	Helix D	Receptor site III
L168	Helix D	Bundle core packing
F174	Helix D	Bundle core packing
L175	Helix D	Bundle core packing
L179	Helix D	Bundle core packing
R180	Helix D	Receptor site I
R183	Helix D	Receptor site I

[a] Putative roles for each residue were assigned on the following basis. Residues assigned to ''bundle core packing'' were found to be involved in the interior helical packing of the four-helix bundle. Residues were assigned to specific receptor binding sites on the basis of published mutagenesis data or as defined in the legend to Figure 6.

Figure 5. Ribbon diagram of the heterotrimeric IL-6 receptor complex. The schematic is based upon the X-ray structure of the GH-receptor complex (De Vos *et al.*, 1992) by superposition of the NMR-derived IL-6 structure on GH. IL-6 is shown in green, IL-6Rα in yellow, and gp130 in orange. Receptor binding sites are labeled I, II, and III. Also shown in red CPK are IL-6 residues, one per site, identified as critical for binding to receptor components: site I, R180; site II, Y32; and site III, W158. The top view is obtained by a 90° rotation of the bottom view along the horizontal axis.

inserted in the rodent strains (data not shown). Interestingly, bovine, porcine, and ovine IL-6 may have a shorter A helix given the presence of a Pro four residues into the presumed start of the helix. Despite some interspecies variations, however, the essential features of the tertiary structure of human IL-6 should be retained in all mammalian forms.

Discussion

This study presents the first high-resolution NMR structure of a long-chain four-helix bundle cytokine reported to date. As a protein of 185 amino acid residues with a high α-helical content, IL-6 presents a challenge for NMR-based structure determination. Spectral dispersion, even in multidimensional NMR experiments, was poor and magnetization transfer was problematic, especially in terms of obtaining stereospecific assignments. Nonetheless, a sufficient number of restraints per residue, including a limited number of important stereospecific assignments, allowed the generation of an ensemble of structures with geometric and energetic characteristics that compare very favorably to other NMR-based structure determinations of substantially smaller proteins. The high quality of the NMR-derived structure of IL-6 is due, in no small part, to the intrinsic packing of the long helices into a four-helix bundle, thus compensating for what would otherwise be significant methodological limitations.

The averaged structure from the NMR-derived ensemble relates well to the structures of other long-chain four-helix bundle cytokines, including G-CSF (Zink *et al.*, 1994; Hill *et al.*, 1993), LIF (Robinson *et al.*, 1994), CNTF (McDonald *et al.*, 1995), and GH (Ultsch *et al.*, 1994). The structure of IL-6 retains many of the structural characteristics ascribed to this family of proteins that distinguish them from their short-chain counterparts (e.g. IL-3, IL-4, IL-5, and M-CSF; Sprang & Bazan, 1993). These include the length of helices in the bundle, the presence of short extra-core α-helices instead of extra-core β-sheets, and a characteristic AB over CD loop packing. Within this family, certain structural features distinguish IL-6 from other family members. For example, the extra-core mini-helices of the neuropoietic cytokines LIF and CNTF are localized to the AB loop, whereas these helices are present in the CD loop in IL-6, as in interferon-β (IFN-β) (Senda *et al.*, 1992). In the case of IL-6, one of the two potential N-linked glycosylation sites (at N46 and N145) is located, though not utilized (Orita *et al.*, 1994), within this helix. This is likely

Table 4. Summary of mutagenesis data defining receptor binding sites on select cytokines[a]

Cytokine	Site I Specificity conferring	Site II Accessory-signal transduction	Site III Accessory-signal transduction
IL-6[b]	to IL-6Rα Q176,S177,S178,L179, **R180**,A181,L182,R183	to gp130 **Y32**,G36,S119,V122	to gp130 K47,S48,M50,E52 K55,L59,**W158**, D161,T163
CNTF[c]	to CNTF-Rα R25,R28,Q63,W64, **R171**,R177	to gp130 **K26**,D30	to LIF-R **F152**,K154,W157, G158,E153,K155
LIF[d]	to LIF-R K170,**A174**,V175	to gp130 Q25,S28,**Q32**,D120, I121,G124,S127	to LIF-R P51,D57,P105,T150 K153,D154,A155, **F156**,K158,K159 K102
IL-4[e]	Accessory-signal transduction to IL-2R I11,**R121**,Y124,S125	Specificity conferring to IL-4R E9,S16,Q78,R81,**R85** R88	Specificity conferring to IL-4R L109,**N111**,F112, L116

[a] The three sites were defined topologically as: site I, C terminus of D helix, N terminus of A helix, plus portions of the AB loop; site II, on the A-C helical face; and site III, C terminus of the A helix, N terminus of the D helix, and portions of the AB and CD loops. Mutagenesis data were tabulated from the cited references and associated with one of the three sites. The functional consequence of each mutation was noted from the cited reference. Residues which roughly correspond to the geometric center of all mapped residues for that site are shown in bold.

[b] Mutagenesis data taken from Ciapponi *et al*. (1995); Savino *et al*. (1994a,b); Paonessa *et al*. (1995); Ehlers *et al*. (1994); Brakenhoff *et al*. (1994); de Hon *et al*. (1994, 1995).

[c] Mutagenesis data taken from Panayotatos *et al*. (1995); Thier *et al*. (1995); Inoue *et al*. (1995).

[d] Mutagenesis data taken from Hudson *et al*. (1996); Layton *et al*. (1994).

[e] Mutagenesis data taken from Morrison & Leder, (1992); Kruse *et al*. (1993); Muller *et al*. (1994); Gustchina *et al*. (1995).

due to the fact that N145 is on the face of the E helix interacting with the B helix.

The NMR-determined structure of IL-6 is in good agreement with that determined by X-ray crystallography (Somers *et al*., 1997). As summarized in Table 2 and in Figure 4, a comparison of interhelical distances and angles shows excellent agreement between the average NMR and the X-ray structures. Comparison of per residue RMSD between the two structures is also quite good with the main differences being observation of the entire AB loop and reduced values for C^{α} RMSDs in the short BC loop in the NMR-derived structure. Both methods give comparable values for the B helix kink angle and the helical packing skew angles. However, the NMR-derived structure exhibits discernable kinks in the A and D helices that are less evident in the X-ray structure. These kinks are reminiscent of the A and D helix kinks observed in the structures of the neuropoietic cytokines LIF and CNTF (Robinson *et al*., 1994; McDonald *et al*., 1995) which have been suggested to be important for receptor engagement (McDonald *et al*., 1995). However, it should be noted that the A helix kink in the NMR-derived structure of IL-6 is placed near the end of the helix in contrast to the middle as in both LIF and CNTF.

Mapping interspecies sequence differences onto the structure of IL-6 yields two interesting sets of observations. First, over the range of residues for which structure is observed (residues 20 to 185), 31 residues are absolutely conserved (Table 3). Of these, four are Cys residues comprising two disulfide bonds and 18 others are located within α-helices. As noted in Table 3, most of these latter 18 residues have been implicated either in core helical packing or in receptor binding (see below). The remaining nine conserved residues all lie within the AB crossover loop. No conserved residues are present in the CD loop, except for two in the extracore E helix. In contrast, most gaps observed in the multiple alignment fall in the CD loop prior to the E helix. Since this region has yet to be implicated in receptor binding or in maintaining the four-helix bundle topology, it is at least teleologically satisfying as a locus of interspecies variation without significant structural or functional consequence.

The biological effects of IL-6 are mediated through the ordered formation of a heteromeric receptor complex, initiated by the binding of IL-6 to the extracellular domain of IL-6Rα. The IL-6/IL-6Rα complex is then capable of binding gp130. The nature of this complex is thought to be a variation of the GH/GH-receptor paradigm where two receptor molecules bind to GH at distinct sites (Wells & DeVos, 1996). Figure 5 shows a representation of the IL-6 receptor complex based upon this paradigm. In fact, the IL-6 receptor complex is thought

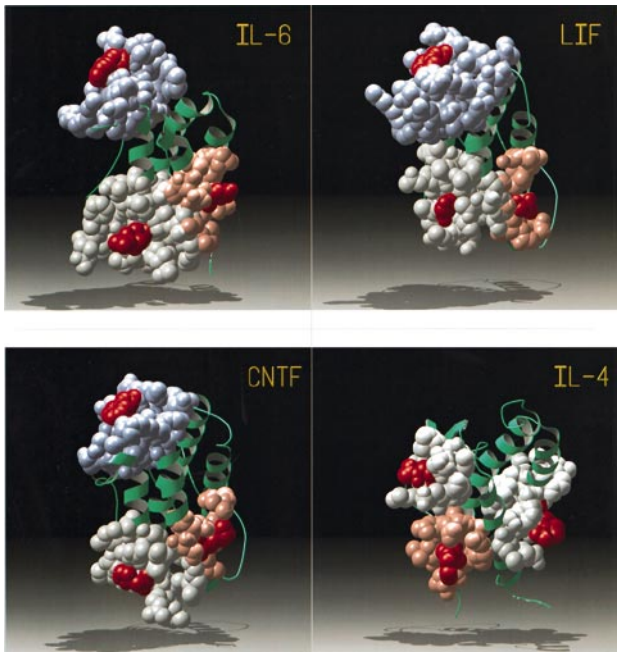

Figure 6. Conservation of topology and functionality of receptor binding sites in four-helix bundle cytokines. Receptor binding sites on IL-6, LIF, CNTF, and IL-4 were generated from published mutagenesis data (Table 4) as described in Methods. The three-dimensional structures of each cytokine were superimposed as described and are viewed from an identical perspective. For all cytokines, the specificity conferring site is shown in white CPK while the accessory sites are shown in pink and blue CPK, respectively. The bold residue for each site listed in Table 4 is shown here in red.

to be hexameric and composed of two molecules each of IL-6, IL-6Rα, and gp130 in accordance with dimerization of gp130 being required for subsequent signal transduction (Paonessa *et al*., 1995). Accordingly, three sites have been designated on IL-6 (Figure 5), which mediate binding to different components of the receptor complex, as determined by a combination of epitope-mapping of antibodies and site-directed mutagenesis (Savino *et al*., 1993, 1994a,b; Paonessa *et al*., 1995; Brakenhoff *et al*., 1995). The determinant for IL-6 binding to IL-6Rα (Savino *et al*., 1993, 1994a,b) is termed site I and is composed of residues at the beginning of the A helix, the C-terminal end of the D helix, and select residues towards the end of the AB loop. Two additional sites (II and III) are responsible for interactions with two different molecules of gp130, only one of which (site II) is strictly analogous to the GH-receptor paradigm (Paonessa *et al*., 1995; Brakenhoff *et al*., 1995). Site II is composed largely of residues in helices A and C while site III, which binds to a gp130 molecule in the opposing heterotrimeric complex, is composed of residues at the amino terminus of the AB loop, at the carboxy terminus of the CD loop (just after the end of helix E) and at the N terminus of the D helix. It is of interest to note that a portion of site III includes residues which, as determined by NMR, are located within a highly mobile region of the AB loop (see Figure 1).

It is clear that other cytokines also utilize at least three sites on their surface for receptor engagement. Indeed, Panayotatos *et al*. (1995) have proposed that long-chain helical cytokines which form heteromeric receptor complexes share a common topological fold and a conserved spatial arrangement of receptor binding sites. Moreover, the functionality associated with each site, in terms of the type of receptor component bound, is also conserved. Thus, the specificity-conferring site I is proposed to be topologically equivalent in CNTF and LIF when mapped onto the available X-ray structures. Sites II and III, which bind the accessory (signal transducing) receptor components gp130 and LIF-R, are similarly conserved. This hypothesis was also extended to IL-6 utilizing a model derived by homology to G-CSF. This hypothesis is potentially important, since a common disposition of functionally equivalent receptor sites would require a similar mechanism of receptor engagement.

The high resolution NMR structure of IL-6 provides additional experimental support for this hypothesis. Moreover, we have also been able to extend this hypothesis to a short-chain cytokine, IL-4, which also employs a heteromeric receptor complex. Table 4 summarizes the available mutagenesis data which define sites I, II, and III in IL-6, LIF, CNTF, and IL-4. Figure 6 illustrates the results of mapping these data onto the available structures (as described in Methods) and shows the conserved spatial disposition of the three sites. Figure 6 also illustrates that the functionality associated with each site is conserved in the long-chain cytokines but reversed in IL-4. The receptor binding sites in IL-4 are more closely spaced, which may be due to the shorter helical lengths. Together, the apparent topological conservation of receptor binding sites, within both short-chain and long-chain cytokines, strongly suggests a divergent evolutionary progression of cytokines and their receptors, as opposed to convergence to common tertiary motifs.

Methods

NMR spectroscopy

A 1.3 mM sample of purified and uniformly ^{15}N or $^{15}N,^{13}C$-labeled recombinant IL-6 was prepared in 10 mM 2-(*N*-morpholino)ethanesulfonic acid (Mes, pH 6.1), 200 mM $MgSO_4$, as described previously (Xu *et al*., 1996). All NMR experiments were performed in 10% ^2H_2O/90% H_2O, except for the 4D $^{13}C,^{13}C$ edited nuclear Overhauser enhancement spectroscopy (NOESY) experiment, which was performed in 100% ^2H_2O. A complete set of NMR resonance assignments, secondary structure analysis, and a gross topology for IL-6 have been reported (Xu *et al*., 1996). Distances restraints were obtained from the analysis of data from a battery of experiments including 2D $^1H,^1H$ NOESY (aromatic re-

gion only), 3D ^{15}N edited NOESY, simultaneous $^{15}N/^{13}C$ edited NOESY (at 100 ms mixing time), and 4D $^{13}C,^{13}C$ edited NOESY experiments (Clore *et al.*, 1991; Zuiderweg *et al.*, 1991; Vuister *et al.*, 1993; Pascal *et al.*, 1994; Xu *et al.*, 1995). Two-dimensional heteronuclear multiple quantum coherence (2D HMQC) *J* experiments (Kay & Bax, 1990) were performed to measure backbone $^3J_{HN\text{-}H^\alpha}$ values and thus define ϕ angle restraints. 3D HNHA *J* experiments (Vuister & Bax, 1993; Garrett *et al.*, 1994) were carried out to confirm and expand the number of ϕ angle restraints. Hydrogen bonds were determined from a series of 2D heteronuclear single quantum coherence (HSQC) experiments after redissolving a sample of lyophilized IL-6 in ^2H_2O and monitoring over time. A combination of 2D constant time (Powers *et al.*, 1991) methyl-relay (L. E. Kay *et al.*, unpublished results), 3D long-range $^{13}C-^{13}C$ *J* coupling (CCJ) (Bax *et al.*, 1992, 1994), 3D ^{15}N edited NOESY, and 4D $^{13}C,^{13}C$ edited NOESY (Clore *et al.*, 1991; Zuiderweg *et al.*, 1991; Vuister *et al.*, 1993) experiments were used to obtain δ-methyl stereospecific assignments for leucine residues. Triple resonance experiments that ultimately detect NH magnetization were recorded using enhanced sensitivity pulse field gradient methods (Muhandiram & Kay, 1994; Kay, 1995). Quadrature detection in all of the indirectly detected dimensions was achieved *via* States time-proportional phase incrementation (TPPI). All data were processed with nmrDraw and nmrPipe programs (Delaglio *et al.*, 1995) and all spectra were extended in the heteronuclear dimensions by forward-backward linear prediction (Zhu & Bax, 1992) prior to apodization and zero filling to double the time domain data points. For HMQC *J* experiments, Varian VNMR software was employed for spectral processing. All data analysis, spectra peak picking and plotting were performed with the psc and pipp programs (Garrett *et al.*, 1991; D. S. Garrett, unpublished results)

Stereospecific assignments of the δ-methyl groups of leucine residues were obtained as follows: First, a 3D long-range CCJ experiment was used where δ-methyl cross-peak intensities are dependent upon $^3J_{C^\alpha\text{-}C^\delta}$ according to the equation:

$$| I_{cross}/I_{diag} |^{1/2} = \tan(2\pi\tau\ ^3J_{C^\alpha\text{-}C^\delta})$$

and $2\tau = 1/^1J_{CC} = 29.4$ ms)(Bax *et al.*, 1994). Using this equation, the χ_2 torsion angle restraints were grouped in two sets ($180^\circ/+60^\circ$ and -60°). Next, a set of peak intensities from a series of NOESY spectra (Powers *et al.*, 1993; Vuister *et al.*, 1993; Pascal *et al.*, 1994; Xu *et al.*, 1995) were derived for these δ-methyl groups, used to assign weak, medium, and strong NOEs, and finally derive stereospecific assignments as described by Powers *et al.* (1993).

Distance restraints were obtained from 3D ^{15}N and 3D/4D ^{13}C heteronuclear-edited NOESY experiments (100 ms mix time) as well as from 2D $^1H,^1H$ NOESY experiments (evaluated in the aromatic region only). Cross-peak intensities were classified as strong, medium and weak using contour levels for calibration with the corresponding distance restraints of 1.8 to 2.7 Å , 1.8 to 3.3 Å , and 1.8 to 5.0 Å, respectively. The lower bound for interproton distances was set to 1.8 Å, which is the sum of the van der Waals (vdW) radii of two protons. The upper distance restraints were further modified for methyl, non-stereospecific methylene or aromatic protons as described (Wüthrich, 1986). Thus, the latter three groups were replaced by the appropriate pseudoatoms and corrected for center averaging. An additional 0.5 Å was added to the upper limit for methyl protons to account for spectral intensity differences (Clore *et al.*, 1987; Wagner *et al.*, 1987).

$J_{HN\text{-}H^\alpha}$ coupling constants from 2D HMQC *J* and 3D HNHA *J* experiments were extracted using the program described by Forman-Kay *et al.* (1990) or that described by Vuister & Bax (1993). Values less than 5 Hz were assigned as $-30^\circ < \phi < -90^\circ$ torsion angle restraints. Values larger than 8 Hz were assigned as $-60^\circ < \phi < -180^\circ$ torsion angle restraints

Structure calculations and refinement

NMR structure refinements and analysis were carried out using X-PLOR version 3.1 (Brünger, 1993) with topallhdg.pro and parallhdg.pro as the topology and parameter sets, respectively. The standard NMR refinement protocol recommended in X-PLOR was followed. This included three stages: (1) partial substructure distance geometry embedding to generate 75 initial structures; (2) simulated annealing starting at a temperature of 2000 K with variably scaled force constants and parameters to a final temperature of 100 K; (3) refinement by further simulated annealing starting at 1000 K with 2000 cooling steps to a final temperature of 100 K and a final scaling of 0.78 for the vdW radii. This protocol gave only two structures that showed no NOE distance violation greater than 0.3 Å and no dihedral angle violation greater than five degrees. To increase the number of such acceptable structures, the refinement was continued with a gentle cycle of simulated annealing that started with a temperature of 300 K, slowly cooling down to 100 K in 20,000 steps. Such refinement yielded an ensemble of 32 structures that showed no NOE distance violation greater than 0.3 Å and no dihedral angle violation greater than five degrees. The Aqua/Procheck-NMR suite of programs (Laskowski *et al.*, 1996) was then used to identify 14 remaining NOE violations (all less than 0.3 Å) common to the ensemble. These restraints were ''loosened'' in their categorization one level and a final cycle of refinement was performed yielding the final set of 32 structures. Main-chain N, C, and C^α atoms of the 105 residues defining the core four-helix bundle (see the text) were superimposed and an average structure was then derived from averaging the Cartesian coordinates. The average structure was subjected to 1000 steps of Powell minimization using X-PLOR (Brünger, 1993). The final average and minimized structure has only one NOE violation greater than 0.3 Å and no dihedral angle violations greater than five degrees.

Other techniques

Multiple sequence alignments were performed according to Needleman & Wunch (1970) and Feng & Doolittle (1987) as implemented in QUANTA96 (Molecular Simulation, Inc.). Raytraced images were generated using the RAYSCRIPT patch (D. and E. Peisach, Brandeis University, personal communication) to MOLSCRIPT (Kraulis, 1991) with subsequent rendering with the program RAYSHADE (C. Kolb, Stanford University). The algorithm of Chothia *et al.* (1981) as implemented in CHARMM (Brooks *et al.*, 1983) was used to analyze the packing of the helices in the refined structures.

Binding sites on IL-6, CNTF, LIF, and IL-4 for their respective receptor components were defined as follows.

The structure of human CNTF was constructed with the homology modeling package MODELER (Sali *et al.*, 1995) based on the X-ray structure of murine LIF (Robinson *et al.*, 1994) and the sequence alignment of McDonald *et al.* (1995). The structures of murine LIF and human IL-4 were from the Brookhaven Protein Data Bank (accession numbers 1LKI and 1BBN, respectively). The structures of the cytokines were first superimposed according to the method of Sutcliffe *et al.* (1987), as implemented in QUANTA, with the IL-6 structure as the target. For each cytokine, all residues identified by site-directed mutagenesis as important for receptor binding were tabulated as in Table 4 and mapped onto the appropriate structure and visualized using the program VMD (Humphrey *et al.*, 1996). A mapped residue centrally located within this subset of the molecular surface was then manually selected and a search performed, using the program RIBBONS (Carson, 1991) to define the minimum distance from this residue which encompasses all mapped residues for the site. Typically, the binding site was then defined by all atoms included within the area of the molecular surface inclusive of this distance from the central residue. However, if too few mutations were available, the distance derived for an analogous site on a related cytokine was employed. Thus, these receptor binding sites are only a crude approximation of the actual receptor sites.

Acknowledgements

We thank Drs Francis Sullivan and Désirée Tsao (Genetics Institute) as well as Martin Karplus (Harvard University) for critical readings of this manuscript and for many helpful suggestions.

References

Bax, A., Max, D. & Zax, D. (1992). Measurement of long-range ^{13}C-^{13}C *J* couplings in a 20-kDa protein-peptide complex. *J. Am. Chem. Soc.* **114**, 6924.

Bax, A., Delaglio, F., Grzesiek, S. & Vuister, G., W. (1994). Resonance assignment of methionine methyl groups and χ3 angular information from long-range proton-carbon and carbon-carbon *J* correlation in a calmodulin-peptide complex. *J. Biomol. NMR.* **4**, 787–797.

Brakenhoff, J. P., de Hon, F. D., Fontaine, V., ten Boekel, E., Schooltink, H., Rose-John, S., Heinrich, P. C., Content, J. & Aarden, L. A. (1994). Development of a human interleukin-6 receptor antagonist. *J. Biol. Chem.* **269**, 86–93.

Brakenhoff, J. P., de Hon, F. D. & Aarden, L. A. (1995). Development of human IL-6 receptor antagonists. *Ann. NY Acad. Sci.* **762**, 129–134.

Brooks, B. R., Bruccoleri, R. E., Olafson, B. D., States, D. J., Swaminathan, S. & Karplus, M. (1983). CHARMM: a program for macromolecular energy, minimization, and dynamics calculations. *J. Comput. Chem.* **4**, 187–217.

Brünger, A. T. (1993). In *X-PLOR Version 3.1: A System for X-ray Crystallography and NMR.* Yale University Press, New Haven, CT.

Carson, M. (1991). Ribbons 2.0. *J. Appl. Crystallog.* **24**, 958–961.

Chothia, C., Levitt, M. & Richardson, D. (1981). Helix to helix packing in proteins. *J. Mol. Biol.* **145**, 215–250.

Ciapponi, L., Graziani, R., Paonessa, G., Lahm, A., Ciliberto, G. & Savino, R. (1995). Definition of a composite binding site for gp130 in human interleukin-6. *J. Biol. Chem.* **270**, 31249–31254.

Clore, G. M., Gronenborn, A. M., Nilges, M. & Ryan, C. A. (1987). Three-dimensional structure of potato carboxypeptidase inhibitor in solution. A study using nuclear magnetic resonance, distance geometry, and restrained molecular dynamics. *Biochemistry,* **26**, 8012–8013.

Clore, G. M., Kay, L. E., Bax, A. & Gronenborn, A. M. (1991). High-resolution three-dimensional structure of interleukin 1 beta in solution by three- and four dimensional nuclear magnetic resonance spectroscopy. *Biochemistry,* **30**, 12–18.

Davis, S., Aldrich, T. H., Stahl, N., Pan, L., Taga, T., Kishimoto, T., Ip, N. Y. & Yancopoulos, G. D. (1993). LIFRβ and gp130 as heterodimerizing signal transducers of the tripartite CNTF receptor. *Science,* **260**, 1805–1808.

de Hon, F. D., Ehlers, M., Rose-John, S., Ebeling, S. B., Bos, H. K., Aarden, L. A. & Brakenhoff, J. P. (1994). Development of an interleukin (IL) 6 receptor antagonist that inhibits IL-6-dependent growth of human myeloma cells. *J. Expt. Med.* **180**, 2395–2400.

de Hon, F. D., ten Boekel, E., Herrman, J., Clement, C., Ehlers, M., Taga, T., Yasukawa, K., Ohsugi, Y., Kishimoto, T., Rose-John, S., Wijdenes, J., Kastelein, R., Aarden, L. A. & Brakenhoff, J. P. (1995). Functional distinction of two regions of human interleukin 6 important for signal transduction via gp130. *Cytokine,* **7**, 398–407.

Delaglio, F., Grzesiek, S., Vuister, G. W., Zhu, G., Pfeifer, J. & Bax, A. (1995). NMRPipe: a multidimensioanl spectral processing system based on UNIX pipes. *J. Biomol. NMR,* **6**, 277–293.

De Vos, A. M., Ultsch, M. & Kossiakoff, A. A. (1992). Human growth hormone and extracellular domain of its receptor: crystal structure of the complex. *Science,* **255**, 306–312.

Ehlers, M., Grotzinger, J., deHon, F. D., Mullberg, J., Brakenhoff, J. P., Liu, J., Wollmer, A. & Rose-John, S. (1994). Identification of two novel regions of human il-6 responsible for receptor binding and signal transduction. *J. Immunol.* **153**, 1744–1753.

Feng, D. F. & Doolittle, R. F. (1987). Progressive sequence alignment as a prerequisite to correctphylogenetic trees. *J. Mol. Evol.* **25**, 351–360.

Forman-Kay, J. D., Gronenborn, A. M., Kay, L. E., Wingfield, P. T. & Clore, G. M. (1990). Studies on the solution conformation of human thioredoxin using heteronuclear ^{15}N-^{1}H nuclear magnetic resonance spectroscopy. *Biochemistry,* **29**, 1566–1572.

Garrett, D. S., Powers, R., Gronenborn, A. M. & Clore, G. M. (1991). A common sense approach to peak picking in two-, three-, and four-dimensional spectra using automatic computer analysis of contour diagrams. *J. Magn. Reson.* **95**, 214–220.

Garrett, D. S., Kuszewski, J., Hancoca, T. J., Lodi, P. J., Vuister, G. W., Gronenborn, A. M. & Clore, G. M. (1994). The impact of direct refinement against three-bond HN-CαH coupling constants on protein structure determination by NMR. *J. Magn. Reson. ser. B,* **104**, 99–103.

Gustchina, A., Zdanov, A., Schalk-Hihi, C. & Wlodawer, A. (1995). A model of the complex between inter-

leukin-4 and its receptors. *Proteins: Struct. Funct. Genet.* **21**, 140–148.

Hill, C. P., Osslund, T. D. & Eisenberg, D. (1993). The structure of granulocyte-colony-stimulating factor and its relationship to other growth factors. *Proc. Natl Acad. Sci., USA,* **90**, 5167–5171.

Hirano, T., Yasukawa, K., Harada, H., Taga, T., Watanabe, Y., Matsuda, T., Kashiwamura, S., Nakajima, K., Koyama, K., Iwamatsu, A., Tsunasawa, S., Sakiyama, F., Matsui, H., Takahara, Y., Taniguchi, T. & Kishimoto, T. (1986). Complementary DNA for a novel human interleukin (BSF-2) that induces lymphocytes to produce immunoglobulin. *Nature,* **324**, 73–76.

Hirano, T., Akira, S., Taga, T. & Kishimoto, T. (1990). Biological and clinical aspects of interleukin 6. *Immunol. Today,* **11**, 443–449.

Hudson, K. R., Vernallis, A. B. & Heath, J. K. (1996). Characterization of the receptor binding sites of human leukemia inhibitory factor and the creation of antagonists. *J. Biol. Chem.* **271**, 11971–11978.

Humphrey, W., Dalke, A. & Schulten, K. (1996). VDM: visual molecular dynamics. *J. Mol. Graph.* **14**, 33–38.

Inoue, M., Nakayama, C., Kikuchi, K., Kimura, T., Ishige, Y., Ito, A., Kanaoka, M. & Noguchi, H. (1995). D1 cap region involved in the receptor recognition and neural cell survival activity of human ciliary neurotrophic factor. *Proc. Natl Acad. Sci. USA,* **92**, 8579–8583.

Ishimi, Y., Miyaura, C., Jin, C. H., Akatsu, T., Abe, E., Nakamura, Y., Yamaguchi, A., Yoshiki, S., Matsuda, T., Hirano, T., Kishimoto, T. & Suda, T. (1990). IL-6 is produced by osteoblasts and induces bone resorption. *J. Immunol.* **145**, 3297–3303.

Ivashkiv, L. B. (1995). Cytokines and STATs: how can signals achieve specificity? *Immunity,* **3**, 1–14.

Kawano, M., Hirano, T., Matsuda, T., Taga, T., Horii, Y., Iwato, K., Asaoku, H., Tang, B., Tanabe, O. & Tanaka, H. (1988). Autocrine generation and requirement of BSF-2/IL-6 for human multiple myelomas. *Nature,* **332**, 83–85.

Kay, L. E. (1995). Pulsed field gradient multi-dimensional NMR methods for the study of protein structure and dynamics in solution. *Prog. Biophys. Mol. Biol.* **63**, 110–126.

Kay, L. E. & Bax, A. (1990). New methods for the measurement of NH-CαH coupling constants in ^{15}N-labeled proteins. *J. Magn. Reson.* **86**, 110–126.

King, D. P., Schrenzel, M. D., McKnight, M. L., Reidarson, T. H., Hanni, K. D., Stott, J. L. & Ferrick, D. A. (1995). Molecular cloning and sequencing of interleukin 6 cDNA fragments from the harbor seal (*Phoca vitulina*), killer whale (*Orcinus orca*), and Southern sea otter (*Enhydra lutris nereis*). *Immunogentics,* **43**, 190–195.

Kishimoto, T. (1989). The biology of interleukin-6. *Blood,* **74**, 1–10.

Kishimoto, T., Akira, S. & Taga, T. (1992). Interleukin-6 and its receptor: a paradigm for cytokines. *Science,* **258**, 593–597.

Kraulis, P. J. (1991). MOLSCRIPT: a program to produce both detailed and schematic plots of protein structures. *J. Appl. Crystallog.* **24**, 946–950.

Kruse, N., Shen, B. J., Arnold, S., Tony, H. P., Muller, T. & Sebald, W. (1993). Two distinct functional sites of human interleukin 4 are identified by variants impaired in either receptor binding or receptor activation. *EMBO J.* **12**, 5121–5129.

Laskowski, R. A., MacArthur, M. W., Moss, D. S. & Thornton, J. M. (1993). PROCHECK: a program to check the stereochemical quality of protein structures. *J. Appl. Crystallog.* **26**, 283–291.

Laskowski, R. A., Rullman, J. A. C., MacArthur, M. W., Kaptein, R. & Thorton, J. M. (1996). ''AQUA and PROCHECK-NMR: Programs for checking the quality of protein structures solved by NMR. *J. Biomol. NMR,* **8**, 477–486.

Layton, M. J., Owczarek, C. M., Metcalf, D., Clark, R. L., Smith, D. K., Treutlein, H. R. & Nicola, N. A. (1994). Conversion of the biological specificity of murine to human leukemia inhibitory factor by replacing 6 amino acid residues. *J. Biol. Chem.* **269**, 29891–29896.

Mawatari, M., Kohno, K., Mizoguchi, H., Matsuda, T., Asoh, K., Van Damme, J., Welgus, H. G. & Kuwano, M. (1989). Effects of tumor necrosis factor and epidermal growth factor on cell morphology, cell surface receptors, and the production of tissue inhibitor of metalloproteinases and IL-6 in human microvascular endothelial cells. *J. Immunol.* **143**, 1619–1627.

McDonald, N. Q., Panayotatos, N. & Hendrickson, W. A. (1995). Crystal structure of dimeric human ciliary neurotrophic factor determined by MAD phasing. *EMBO J.* **14**, 2689–2699.

Morrison, B. W. & Leder, P. (1992). A receptor binding domain of mouse interleukin-4 defined by a solid-phase binding assay and *in vitro* mutagenesis. *J. Biol. Chem.* **267**, 11957–11963.

Mott, H. R. & Campbell, I. D. (1995). The solution structure of the F42A mutant of human interleukin 2. *Curr. Opin. Struct. Biol.* **5**, 114–121.

Muhandiram, D. R. & Kay, L. E. (1994). Gradient-enhanced triple-resonance three-dimensional NMR experiments with improved sensitivity. *J. Magn. Reson. ser. B,* **103**, 203–216.

Muller, T., Dieckmann, T., Sebald, W. & Oschkinat, H. (1994). Aspects of receptor binding and signalling of interleukin-4 investigated by site-directed mutagenesis and NMR spectroscopy. *J. Mol. Biol.* **237**, 423–436.

Murakami, M., Hibi, M., Nakagawa, N., Nakagawa, T., Yasukawa, K., Yamanishi, K., Taga, T. & Kishimoto, T. (1993). IL-6-induced homodimerization of gp130 and associated activation of a tyrosine kinase. *Science,* **260**, 1808–1810.

Needleman, S. B. & Wunch, C. D. (1970). A general method applicable to the search for similarities in the amino acid sequence of two proteins. *J. Mol. Biol.* **48**, 443–453.

Nilges, M., Clore, G. M. & Gronenborn, A. M. (1988). Determination of three-dimensional structures of proteins from interproton distance data by dynamical simulated annealing from a random array of atoms. Circumventing problems associated with folding. *FEBS Letters,* **229**, 317–324.

Orita, T., Oh-eda, M., Hasegawa, M., Kuboniwa, H., Esaki, K. & Ochi, N. (1994). Polypeptide and carbohydrate structure of recombinant human interleukin-6 produced in Chinese hamster ovary cells. *J. Biochem.* **115**, 345–350.

Panayotatos, N., Radziejewska, E., Acheson, A., Somogyi, R., Thadani, A., Hendrickson, W. A. & McDonald, N. Q. (1995). Localization of functional receptor epitopes on the structure of ciliary neurotrophic factor indicates a conserved, function-re-

lated epitope topography among helical cytokines. *J. Biol. Chem.* **270**, 14007–14014.

Paonessa, G., Graziani, R., De Serio, A., Savino, R., Ciapponi, L., Lahm, A., Salvati, A. L., Toniatti, C. & Ciliberto, G. (1995). Two distinct and independent sites on IL-6 trigger gp130 dimer formation and signalling. *EMBO J.* **14**, 1942–1951.

Pascal, S. M., Muhandiram, D. R., Yamazaki, T., Forman-Kay, J. D. & Kay, L. E. (1994). Nuclear magnetic resonance structure of an SH2 domain of phospholipase C-gamma 1 complexed with a high affinity binding peptide. *J. Magn. Reson. ser. B,* **103**, 197–201.

Powers, R., Gronenborn, A. M., Clore, G .M. & Bax, A. (1991). Three dimensional triple resonance NMR of 13C/15N enriched proteins using constant time evolution. *J. Magn. Reson.* **94**, 209–213.

Powers, R., Garrett, D. S., March, C. J., Frieden, E. A., Gronenborn, A. M. & Clore, G. M. (1993). The high-resolution, three-dimensional solution structure of human interleukin-4 determined by multidimensional heteronuclear magnetic resonance spectroscopy. *Biochemistry,* **32**, 6744–6752.

Robinson, R. C., Grey, L. M., Staunton, D., Vankelecom, H., Vernallis, A. B., Moreau, J. F., Stuart, D. I., Heath, J. K. & Jones, E. Y. (1994). The crystal structure and biological function of leukemia inhibitory factor: implications for receptor binding. *Cell,* **77**, 1101–1116.

Sali, A., Potterton, L., Yuan, F., van Vlijmen, H. & Karplus, M. (1995). Evaluation of comparative protein modeling by MODELLER. *Proteins: Struct. Funct. Genet.* **23**, 318–326.

Savino, R., Lahm, A., Giorgio, M., Cabibbo, A., Tramontano, A. & Ciliberto, G. (1993). Saturation mutagenesis of the human interleukin 6 receptor binding site: implications for its three dimensional structure. *Proc. Natl Acad. Sci., USA,* **90**, 4067–4071.

Savino, R., Ciapponi, L., Lahm, A., Demartis, A., Cabibbo, A., Toniatti, C., Delmastro, P., Altamura, S. & Ciliberto, G. (1994a). Rational design of a receptor super-antagonist of human interleukin-6. *EMBO J.* **13**, 5863–5870.

Savino, R., Lahm, A., Salvati, A. L., Ciapponi, L., Sporeno, E., Altamura, S., Paonessa, G., Toniatti, C. & Ciliberto, G. (1994b). Generation of interleukin-6 receptor antagonists by molecular-modeling guided mutagenesis of residues important for gp130 activation. *EMBO J.* **13**, 1357–1367.

Senda, T., Shimazu, T., Matsuda, S., Kawano, G., Shimizu, H., Nakamura, K. T. & Mitsui, Y. (1992). Three-dimensional crystal structure of recombinant murine interferon-beta. *EMBO J.* **11**, 3193–3201.

Somers, W., Stahl, M. & Seehra, J. (1997). 1.9 Å Crystal structure of interleukin 6: implications for a novel mode of receptor dimerisation and signalling. *EMBO J,* **5**, 989–997.

Sprang, S. R. & Bazan, J. F. (1993). Cytokine structural taxonomy and mechanisms of receptor engagement. *Curr. Opin. Struct. Biol.* **3**, 815–827.

Starnes, H. F., Pearce, M. K., Tewari, A., Yim, J. H., Zou, J.-C. & Abrams, J. S. (1990). Anti-IL-6 monoclonal antibodies protect against lethal *Escherichia coli* infection and lethal tumor necrosis factor-alpha challenge in mice. *J. Immunol.* **145**, 4185–4191.

Sutcliffe, M. J., Haneef, I., Carney, D. & Blundell, T. L. (1987). Knowledge-based modeling of homologous proteins. Part I: three-dimensional frameworks derived from the simultaneous superposition of multiple structures. *Protein Eng.* **1**, 377–384.

Taga, T., Hibi, M., Hirata, Y., Yamasaki, K., Yasukawa, K., Matsuda, T., Hirano, T. & Kishimoto, T. (1989). Interleukin-6 triggers the association of its receptor with a possible signal transducer, gp130. *Cell,* **58**, 573–581.

Thier, M., Simon, R., Kruttgen, A., Rose-John, S., Heinrich, P. C., Schroder, J. M. & Weis, J. (1995). Site-directed mutagenesis of human CNTF: functional analysis of recombinant variants. *J. Neurosci. Res.* **40**, 826–835.

Ultsch, M. H., Somers, W., Kossiakoff, A. A. & de Vos, A. M. (1994). The crystal structure of affinity-matured human growth hormone at 2 Å resolution. *J. Mol. Biol.* **236**, 286–299.

Van Damme, J., Opdenakker, G., Simpson, R. J., Rubira, M. R., Cayphas, S., Vink, A., Billiau, A. & Van Snick, J. (1987). Identification of the human 26-kD protein, interferon beta 2 (IFN-beta 2), as a B cell hybridoma/plasmacytoma growth factor induced by interleukin 1 and tumor necrosis factor. *J. Expt. Med.* **165**, 914–919.

Vuister, G. W. & Bax, A. (1993). Quantitative *J* correlation: a new approach for measuring homonuclear three-bond *J*(HN-Hα) coupling constants in ^{1}5N-enriched proteins. *J. Am. Chem. Soc.* **115**, 7772–7777.

Vuister, G. W., Clore, G. M., Gronenborn, A. M., Powers, R., Garrett, D. S., Tschudin, R. & Bax, A. (1993). Increased resolution and improved spectral quality in four-dimensional carbon-13/carbon-13-separated HMQC-NOESY-HMQC spectra using pulsed field gradients. *J. Magn. Reson. ser. B,* **101**, 210–213.

Wagner, G., Braun, W., Havel, T. F., Schaumann, T., Go, N. & Wüthrich, K. (1987). Protein structures in solution by nuclear magnetic resonance and distance geometry. The polypeptide fold of the basic pancreatic trypsin inhibitor determined using two different algorithms, DISGEO and DISMAN. *J. Mol. Biol.* **196**, 611–639.

Ward, L. D., Howlett, G. J., Discolo, G., Yasukawa, K., Hammacher, A., Moritz, R. L. & Simpson, R. J. (1994). High affinity interleukin-6 receptor is a hexameric complex consisting of two molecules each of interleukin-6, interleukin-6 receptor, and gp-130. *J. Biol. Chem.* **269**, 23286–23289.

Wells, J. A. & DeVos, A. M. (1996). Hematopoietic receptor complexes. *Annu. Rev. Biochem.* **65**, 609–634.

Wüthrich, K. (1986). *NMR of Proteins and Nucleic Acids.* John Wiley, New York, NY.

Xu, G. Y., Ong, E., Gilkes, N. R., Kilburn, D. G., Muhandiram, D. R., Harris-Brandts, M., Carver, J. P., Kay, L. E. & Harvey, T. S. (1995). Solution structure of a cellulose-binding domain from *Cellulomonas fimi* by nuclear magnetic resonance spectroscopy. *Biochemistry,* **34**, 6993–7009.

Xu, G. Y., Hong, J., McDonagh, T., Stahl, M., Kay, L. E., Seehra, J. & Cumming, D. A. (1996). Complete ^{1}H, ^{15}N and ^{13}C assignments, secondary structure, and topology of recombinant human interleukin-6. J. *Biomol. NMR.* **8**, 123–135.

Zhu, G. & Bax, A. (1992). Improved linear prediction of damped NMR signals using modified ''forward-backward'' linear prediction. *J. Magn. Reson.* **100**, 202–207.

Zink, T., Ross, A., Luers, K., Cieslar, C., Rudolph, R. & Holak, T. A. (1994). Structure and dynamics of the human granulocyte colony-stimulating factor determined by NMR spectroscopy. Loop mobility in a four-helix-bundle protein. *Biochemistry,* **33**, 8453–8463.

Zuiderweg, E. R., Petros, A. M., Fesik, S. W. & Olejniczak, E. T. (1991). Four-dimensional (^{13}C,^{1}H,^{13}C,^{1}H) HMQC-NOE-HMQC NMR spectroscopy: resolving tertiary nuclear Overhauser effect distance constraints in the spectra of larger proteins. *J. Am. Chem. Soc.* **113**, 370–371.

Edited by P. E. Wright

(Received 16 October 1996; received in revised form 16 January 1997; accepted 21 January 1997)